Tech Science Press

Finite Element Analysis on Vibration Characteristics of an Offshore Floating Breakwater

Hongyi Yan[1], Dingguo Zhang[1], Liang Li[1,*] and Xiaoyu Luo[2]

[1]Nanjing University of Science and Technology, Nanjing, 210094, China
[2]Electric Power Research Institute of Guangdong Power Grid Co., Ltd., Guangzhou, 510080, China
*Corresponding Author: Liang Li. Email: liangli@mail.njust.edu.cn

Abstract: The construction of seaside facilities is a hot topic in the field of ocean engineering. In this paper, a new type of floating breakwater is designed by 3D-CAD geometric modeling. Based on the vibration theory and finite element technology, the floating breakwater model is optimized, and the modal analysis of the structure with the bracket as main body and blades as functional attachments is carried out. Natural frequencies and mode shapes of the blades are first calculated, and the effects of the natural frequencies in both dry and wet conditions are taken into account. Modal analysis and harmonic response analysis of the bracket with different lengths by removing the blades are also carried out, and the different variations of the natural frequencies between several bracket units are compared. The responses of the key position of the bracket under different loads and different bracket lengths are analyzed. The influence of liquid on the natural frequency of the blades and the influence of the length of the bracket on the natural frequency of the bracket are discussed in the fluid-solid coupling state. Research in this paper provides a data basis for the safety assessment of the breakwater construction.

Keywords: Breakwater; modal analysis; fluid-structure interaction; finite element simulation

1 Introduction

The floating breakwaters, which are distinguished from the traditional solid breakwaters, are making up with the floating body and the anchoring system [1, 2]. The floating body can be used to prevent the wave propagation and break the waveform [3]. Furthermore, the movement of the floating body itself can destroy the original motion state of the fluid, thereby achieving the effect of eliminating waves [4, 5]. The floating breakwater was originally built and used by the United Kingdom in Portsmouth in 1811, and China used the floating breakwater for the first time in Danjiangkou Reservoir in 1962 [6]. Because of its potential of rapid construction, low cost, good wave-eliminating effect, being suitable for deep water environment and deepening of marine development, floating breakwaters have begun to be widely used. At the same time, floating breakwaters also have the disadvantages of complex anchoring

systems and collisions between floating bodies [7-9]. Therefore, the design and research of floating breakwaters is particularly important.

Offshore platforms such as floating breakwaters often need to withstand harsh working conditions. To this end, domestic and foreign scholars have conducted a series of studies on floating platforms. In order to prevent the anchoring system from being damaged by the action of wind, waves and current, Liu et al. [10, 11] used the quasi-determined long-term domain method to analyze the motion and dynamic characteristics of the floating platform in the real sea conditions of wind, wave and current; Sun et al. [12] did numerical simulations to study the motion of the semi-submersible platform and checked the mooring line strength. For the platform structure below the water surface subjected to the actions of fluid, the fluid-solid coupling mechanism and responses of vortex-induced vibration of marine flexible structures have been studied extensively [13-16]. For the vibration characteristics of underwater complex stress structures, Yang et al. [17] used polynomial approximation quadratic matrix linearization method based on Flügge shell theory to solve the natural frequency of the structure. Chen et al. [18] studied the influence of aqueous medium on structural vibration modes based on the finite element software, and similar work can be found in Refs. [19, 20]. Jindal et al. [21] presented a theoretical analysis of free dry and wet vibration of a trapezoidal, 2-way tapered, marine spade rudder. Liu et al. [22] investigated the hydrodynamic performance of a submerged two-layer horizontal plate breakwater and obtained an analytical solution for interaction of water waves with the plates.

In this paper, finite element simulation of a new floating breakwater structure is carried out. Parameters of the floating breakwater structure are given in Section 2. In Section 3, the modal analysis of the blades in the structure are done and the effects of natural frequencies of the blades in dry and wet conditions are compared by considering the influence of fluid. In Section 4, modal analysis and resonance response analysis on the bracket structure with the blades removed are carried out, and the variation of the natural frequency of the bracket under different lengths is compared. The responses of the key position of the bracket under different lengths and different stent lengths are analyzed in detail. In Section 5, some conclusions based on the results are drawn.

2 Parameters of Floating Breakwater Structure

The breakwater is composed of two parts, namely an anchoring system and a floating body structure (shown in Figs. 1 and 2). The two ends of the mooring line are respectively attached to the floating body structure and the seabed, and the floating body structure is limited to a specific range to prevent the impact on other normal marine operations. The traditional floating breakwater only relies on the movement of the floating structure to achieve the effect of wave-eliminating, but the new type of breakwater adds a paddle structure to the floating structure. When the fluid passes, the blade rotates,
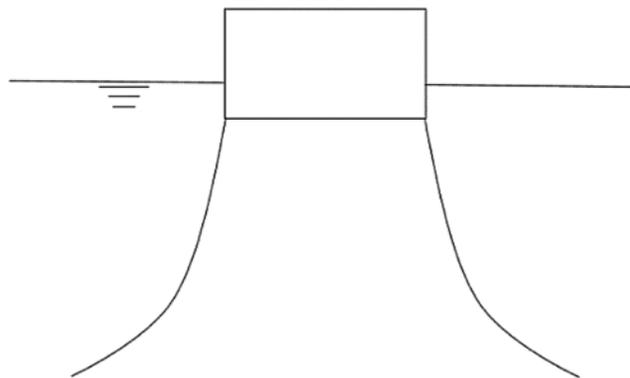
Figure 1: Anchoring system
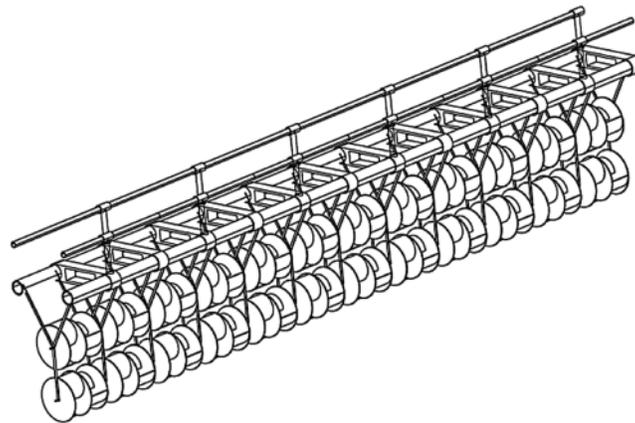
Figure 2: Floating structure
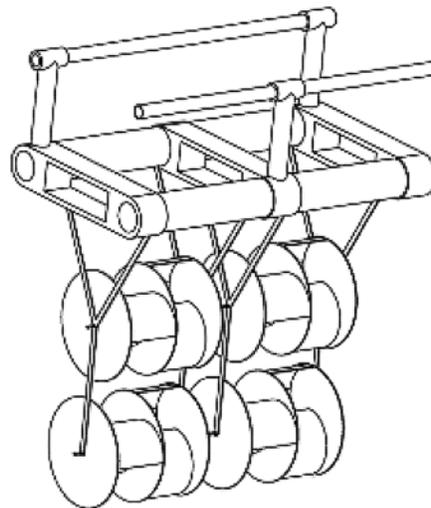
Figure 3: Two unit structure

thereby destroying the movement pattern of the water point to achieve the best wave-eliminating effect. The overall structure of the floating body can be assembled by the unit body composed of two upper and lower blades (Fig. 3 shows a two-unit structure), and the unit body can be decomposed into two parts: the blades and the bracket.

The geometric parameters of the two components are shown in Tabs. 1 and 2, respectively.

Both the blade and the tie rod are made of ordinary carbon steel, the elastic modulus is $2.1e + 011$ Pa, the Poisson ratio is 0.28, the density is 7800 kg/m^3, and the yield strength is $2.206e + 008$ Pa. The components on the remaining brackets are made of PE material, with the physical properties as follows: the elastic modulus is $1.72e + 008$ Pa, the Poisson ratio is 0.439, and the density is 917 kg/m^3.

Table 1: Geometric parameters of blade

Parameters	Actual value/mm
Total Width	1030
Baffle Diameter	1000
Baffle Thickness	10
Blade Radius	300
Blade Width	500
Blade Thickness	10

Table 2: Geometric parameters of bracket (taking two unit bodies as an example)

Parameters	Actual value/mm
Bracket Length	3000
Bracket Outer Diameter	315
Bracket Inner Diameter	269
Beam Width	300
Beam Length	1880
Beam Outer Diameter	380
Railing Outer Diameter	120
Railing Inner Diameter	110
Railing Height	800
Upper Rod Length	1550
Lower Rod Length	1250
Rod Thickness	10
Rod Width	50

3 Blade Modal Analysis

The vibration mode is an inherent, integral property of the elastic structure. Through modal analysis, one can obtain the frequency and modal characteristics of a structure, and judge the actual vibration response of the structure at the susceptible frequency, and it is the basis for complex dynamic analysis. Since the blades are always in the marine fluid environment, the effects of fluids during modal analysis must be taken into account, the process is also known as modal analysis. The effect of fluid on the vibration characteristics of the blade structure is mainly the prestressing effect caused by the load attached to the structure by the fluid and the additional mass effect caused by the vibration of the fluid along with the blade [23].

3.1 Modal Calculation Method in Air

The structural dynamics equation of the structure in air is:

$$[M]\{\ddot{u}\} + [C]\{\dot{u}\} + [K]\{u\} = F(t) \tag{1}$$

where [M] is the mass matrix of the system; [C] is the damping matrix of the system; [K] is the stiffness

matrix of the system; F(t) is the external excitation load; $\{\ddot{u}\}$, $\{\dot{u}\}$, and $\{u\}$ is the acceleration, velocity, and displacement vector of the corresponding node, respectively.

Damping can be ignored in this lightly-damped system in the air. The vibration equation of the system in this case is:

$$[M]\{\ddot{u}\} + [K]\{u\} = \{0\} \tag{2}$$

Equation (2) has the following solutions in the form of simple harmonic motion:

$$\{u(x, y, z, t)\} = \{H(x, y, z)\}e^{t\omega_n t} \tag{3}$$

where $\{H(x, y, z)\}$ is the magnitude of the displacement vector, which defines the spatial distribution of the displacement vector; ω_n is the angular frequency of the simple harmonic motion. Substituting Eq. (3) into Eq. (2), yields:

$$|K - \omega_n^2 M|\{H\}\exp(t\omega_n t) = \{0\} \tag{4}$$

The above formula is established at any time, so it can be removed regardless of the time item:

$$|K - \omega_n^2 M|\{H\} = \{0\} \tag{5}$$

Equation (5) is a typical real eigenvalue problem. $\{H\}$ has a non-zero solution condition:

$$|K - \omega_n^2 M| = 0 \tag{6}$$

or

$$|K - \lambda M| = 0 \tag{7}$$

The left side of Eq. (7) is a λ polynomial, which can solve a set of discrete roots $\lambda_i (i = 1, 2, \ldots, n)$. Substituting Eq. (7) into Eq. (4), one can obtain the corresponding vector $\{H_i\}$, where λ_i is the eigenvalue of the system, and $\{H_i\}$ is the corresponding eigenvector.

3.2 Kinetic Equations in Aqueous Medium

When the system is in an aqueous medium, the Navier-Stokes equation needs to be used. The vibration equation of the system is:

$$M_s \ddot{u} + K_s U = -K_{fs} p \tag{8}$$

where K_{fs} is the stiffness matrix of the fluid acting on the structure; p is the hydroacoustic pressure.

Considering the additional mass and damping of the aqueous medium, it is assumed that the fluid is a non-rotating, non-viscous, uniform compressible fluid, and the fluid pressure is used as an unknown amount to resolve the modality in the aqueous medium. Its three-dimensional wave equation is:

$$\frac{1}{c^2}\frac{\partial^2}{\partial t^2} - \nabla^2 p = 0 \tag{9}$$

where c is the speed of sound in the fluid. Discretize the wave equation yields

$$M_r \ddot{P} + K_f P = F_r \tag{10}$$

Combine Eqs. (10) and (1), one can obtain the kinetic equation of fluid-solid coupling:

$$\begin{bmatrix} M & 0 \\ \rho_f & M_f \end{bmatrix}\begin{bmatrix} \ddot{u} \\ p \end{bmatrix} + \begin{bmatrix} K + K_r & R \\ 0 & K_f \end{bmatrix}\begin{bmatrix} u \\ p \end{bmatrix} = \begin{bmatrix} F_s \\ F_f \end{bmatrix} \tag{11}$$

where the subscript s indicates the solid structure, the subscript f indicates the fluid; Mf, ρf, Kf are the water additional mass matrix, the density matrix, and the additional stiffness matrix, respectively; F_s and F_f are the solid structure matrix and the fluid additional excitation force matrix, respectively; P and $\ddot{P}$ are the fluid particle displacement matrix and acceleration matrix, respectively; R is the fluid-solid coupling condition matrix; K_r is the centrifugal force stiffness matrix.

3.3 Simulation Results

Under the action of waves and ocean currents, the structure will have six degrees of freedom of motion. However, when the shaft is fixed, the blade has only one degree of freedom to rotate around the axis of rotation. In this paper, we only analyze the five degrees of freedom modal except for the rotation around the axis.

The blade model is built in Solidworks and imported into Ansys workbench for material definition, discrete, and mesh division. At the same time, the constraint of only tangential freedom is defined at the axis of rotation, and the dry mode is solved. On this basis, the Acoustic Body command is used to define the fluid domain around the blade structure. The fluid density is 1000 kg/m^3, the sound velocity is 1500 m/s, and the gravitational acceleration is 9.8 m/s^2. Meanwhile, the fluid-solid coupling surface is set, and the pressure freedom of the outer boundary of the fluid domain is zero, so that the internal pressure wave is absorbed when it reaches the outer boundary of the fluid domain. The non-reflective boundary condition is realized, and the infinite flow field will be better simulated.

Table 3 shows the natural frequencies of the blades. It can be seen from Tab. 3 that the natural frequency of the blade in the fluid is smaller than that calculated in the air, which is consistent with the results in literature [24]. This can be explained by the additional mass theory, in which the fluid consumes part of kinetic energy of the blade structure, causing the kinetic energy of the blade to decrease, resulting in a decrease in the natural frequencies of the blades in the fluid [25]. In addition, under each order of vibration, since the magnitude of the work performed by the blade structure on the fluid varies, the natural frequency of the structure itself is affected to varying degrees.

Table 3: Natural frequencies of blade

Order	Natural Frequency/Hz	
	In air	In fluid
1	45.817	27.467
2	56.650	38.575
3	56.756	38.738
4	69.481	40.090
5	82.462	48.984

The first five modes of the blade in the air and in the fluid are shown in Figs. 4 and 5, respectively. It can be seen from Figs. 4 and 5 that the vibration modes of the structure in the fluid are substantially identical to the corresponding vibration modes of the structure in the air, but the vibration amplitude of the structure in the fluid is smaller than that in the air due to the damping of the surrounding fluid.
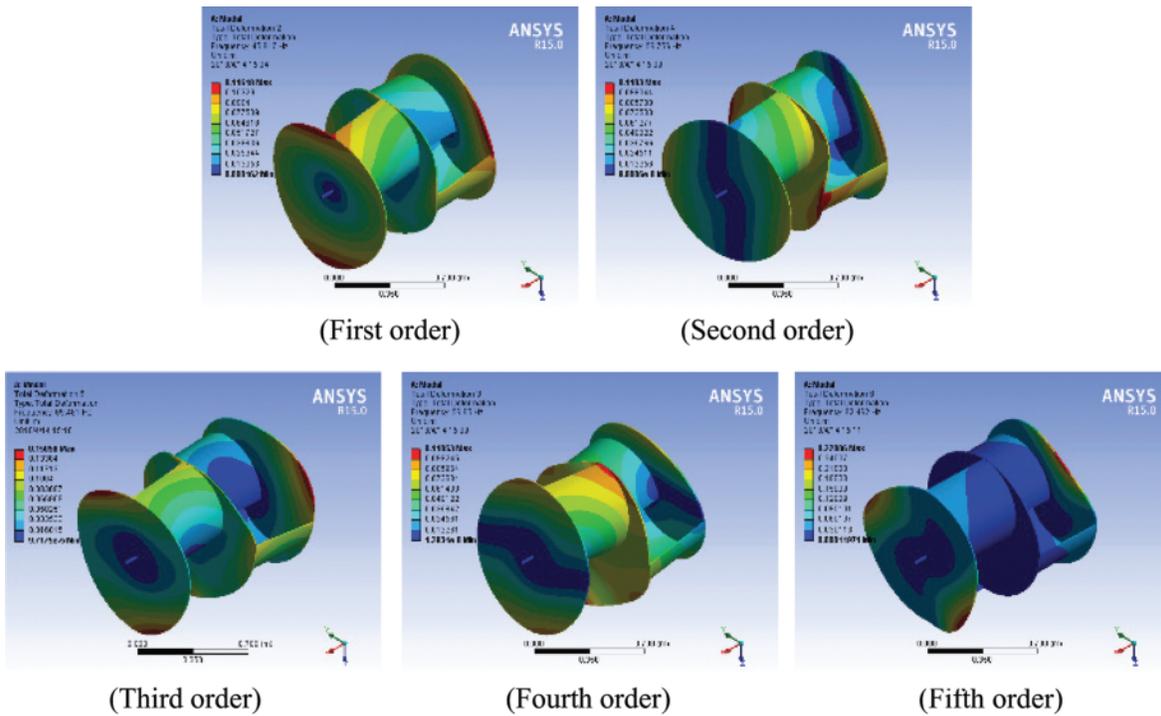
Figure 4: The first five modal modes of the blade (in air)
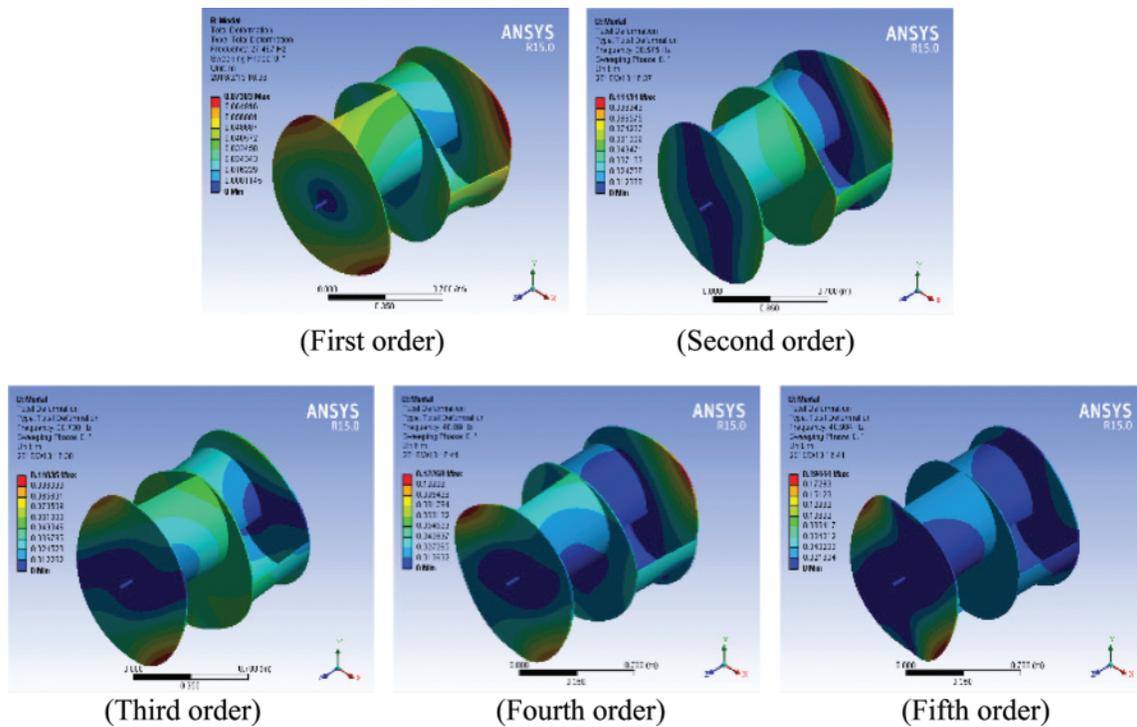
Figure 5: The first five modal modes of the blade (in fluid)

The intersection of the speed-frequency line and the n-th order natural frequency locus is the point where resonance occurs. Fig. 6 shows frequencies of the blade corresponding to rotational speed (Line 1) and natural frequencies of order 1-5. It can be seen from Fig. 6 that the critical blade speeds are: 261.96 rad/s, 278.44 rad/s, 329.52 rad/s, 346.44 rad/s, and 404.62 rad/s. It is impossible for the blade to reach such a high speed under the action of the current, so the blade is unlikely to resonate due to the rotation. In addition, the position with the largest amplitude of the structure is located at the intersection of the baffle and the blade, and the welding method is adopted in the manufacturing process, which is liable to cause structural damage.

4 Bracket Vibration Analysis

4.1 Stent Modal Analysis

Constraints are defined on the anchor structure of the scaffold structure. Fig. 7 shows the fixed constraints on the four anchor points. The modal analysis of the scaffold structures with different cell numbers is performed. In the modal analysis of the stent, we mainly considered the influence of different stent lengths on the vibration characteristics of the structure. The stent structure is appropriately simplified and divided into several components with the same parameters. These constructs can be used to analyze structures with different unit numbers. After meshing, a finite element model is obtained, in
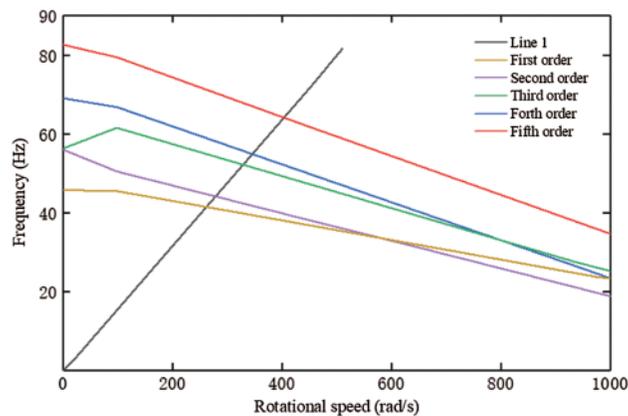
Figure 6: Frequency excited by rotational speed and natural frequency
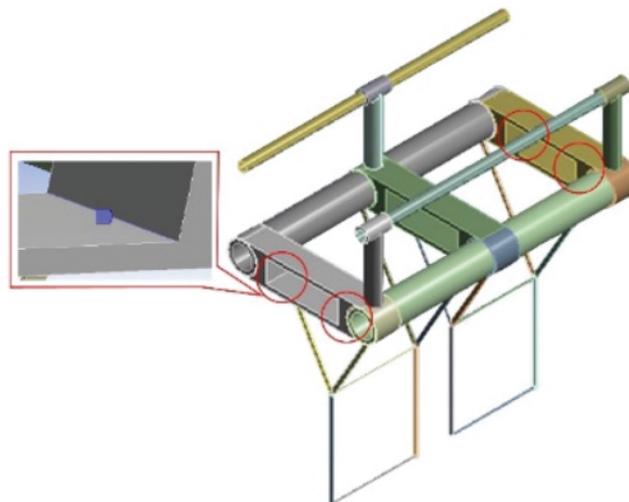
Figure 7: Fixed constraint of four anchor points

which two units have 897,515 nodes, three units have 366,934 nodes, four units have 48,018 nodes, five units have 1,060,244 nodes, six units have 1,527,242 nodes, and seven units have 1,273,416 nodes.

Table 4 shows the resonant frequencies of each order of structure with different unit numbers. It can be seen from Tab. 4 that as the number of support unit bodies increases, the natural frequencies of each order show a downward trend.

Figures 8-13 show the first six mode shapes of the different unit number structures. It can be seen from the structural deformation diagram (Figs. 8-13) that as the lateral span of the bracket increases, the maximum displacement position of the bracket structure is transferred from the railing to the tie rod, the beam and the pipeline. The result is that, as the lateral span of the stent increases, the overall structural flexibility of the stent becomes larger, and the compliance ratio of the railing to the overall structure of the bracket decreases, and the overall structure of the stent is more susceptible to deformation. Considering the actual situation, the tie rod is used

Table 4: Structural resonance frequencies (unit: Hz)

	1st order	2nd order	3rd order	4th order	5th order	6th order
2 units	2.0889	2.1101	2.8106	2.8637	2.9981	3.9503
3 units	2.3071	2.3157	2.3729	2.8332	3.6978	3.7113
4 units	2.1424	2.1958	2.2834	2.3197	2.3983	2.8471
5 units	1.6606	1.9120	2.0657	2.0686	2.0869	2.2074
6 units	1.2326	1.5014	1.9467	1.9897	2.0118	2.0385
7 units	0.95585	1.3480	1.8125	1.9536	2.0471	2.0754

(First order)   (Second order)

(Third order)   (Fourth order)

(Fifth order)   (Sixth order)
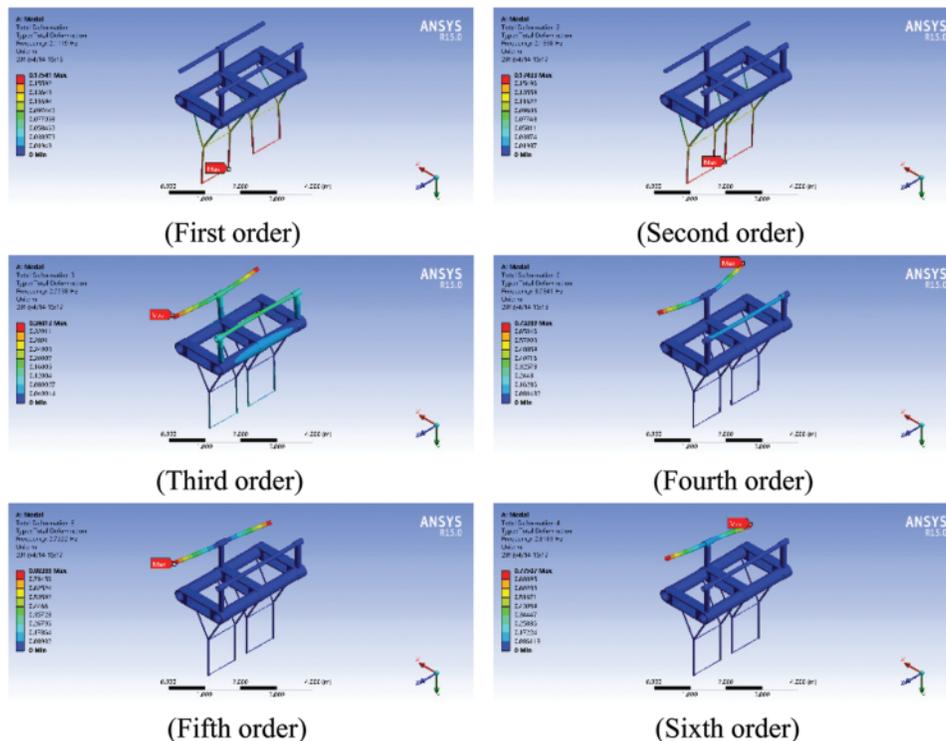
Figure 8: The first six mode shapes of two units structure
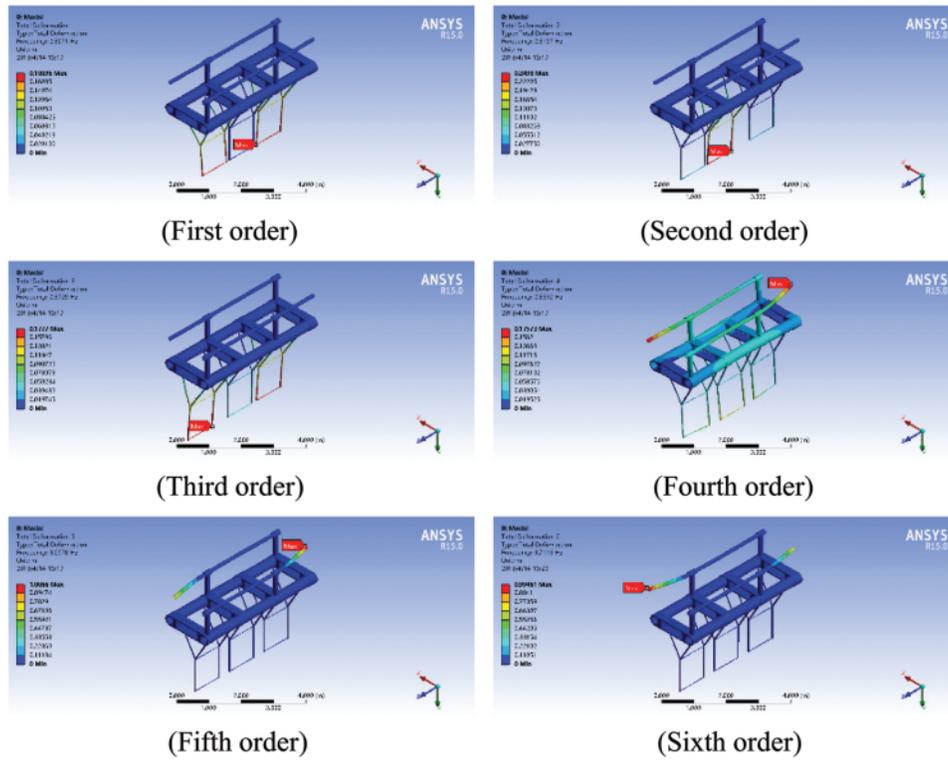
Figure 9: The first six mode shapes of three units structure
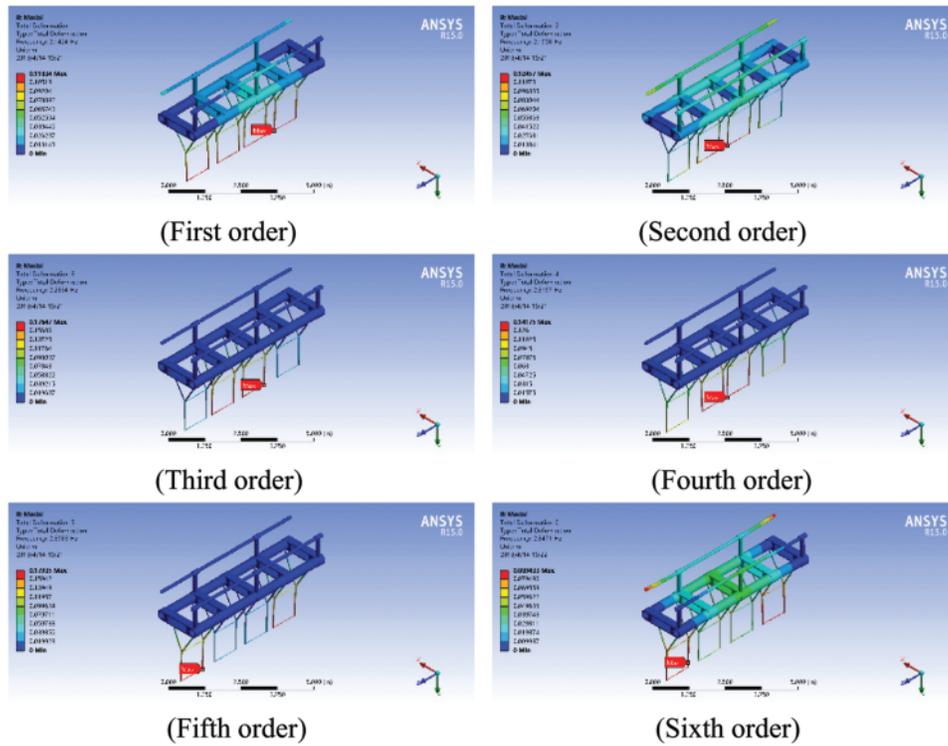
Figure 10: The first six mode shapes of the four units structure
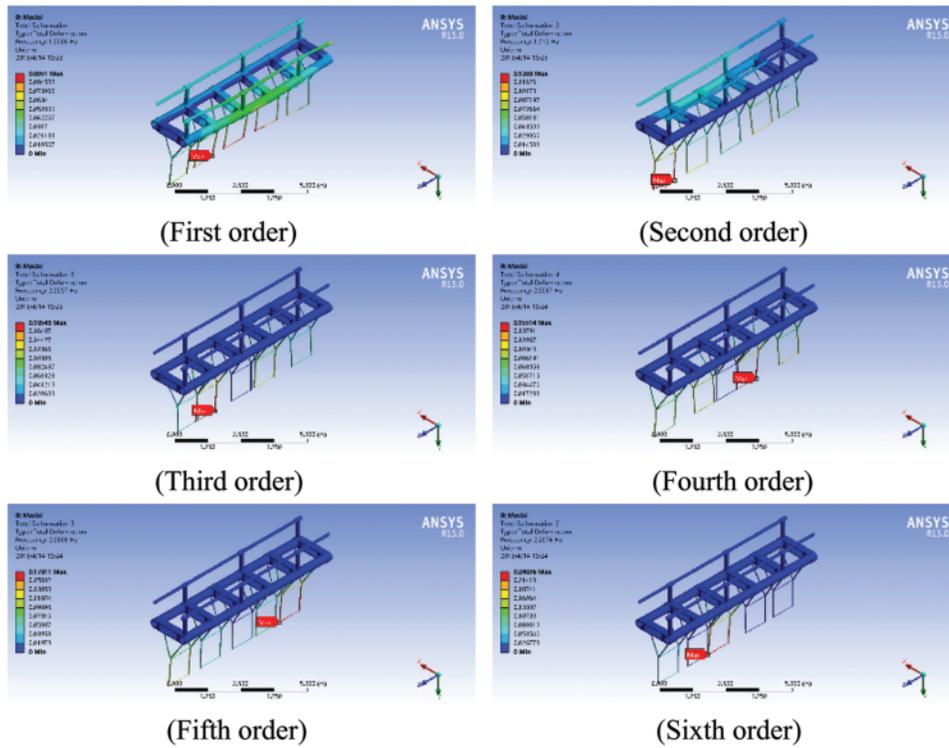
Figure 11: The first six mode shapes of five units structure
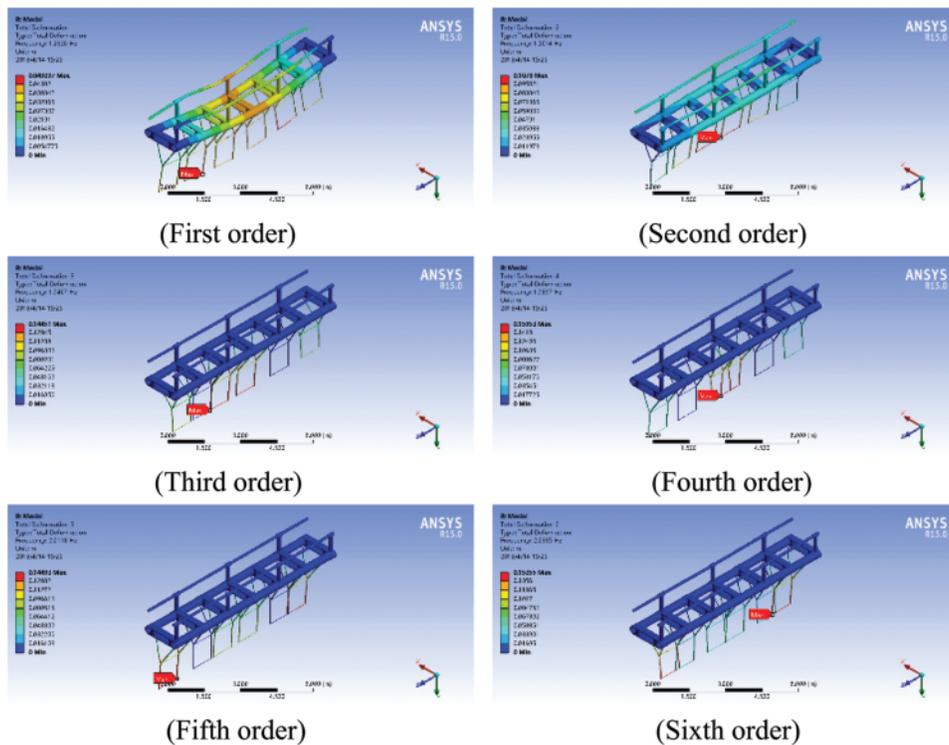
Figure 12: The first six modes of the six units structure
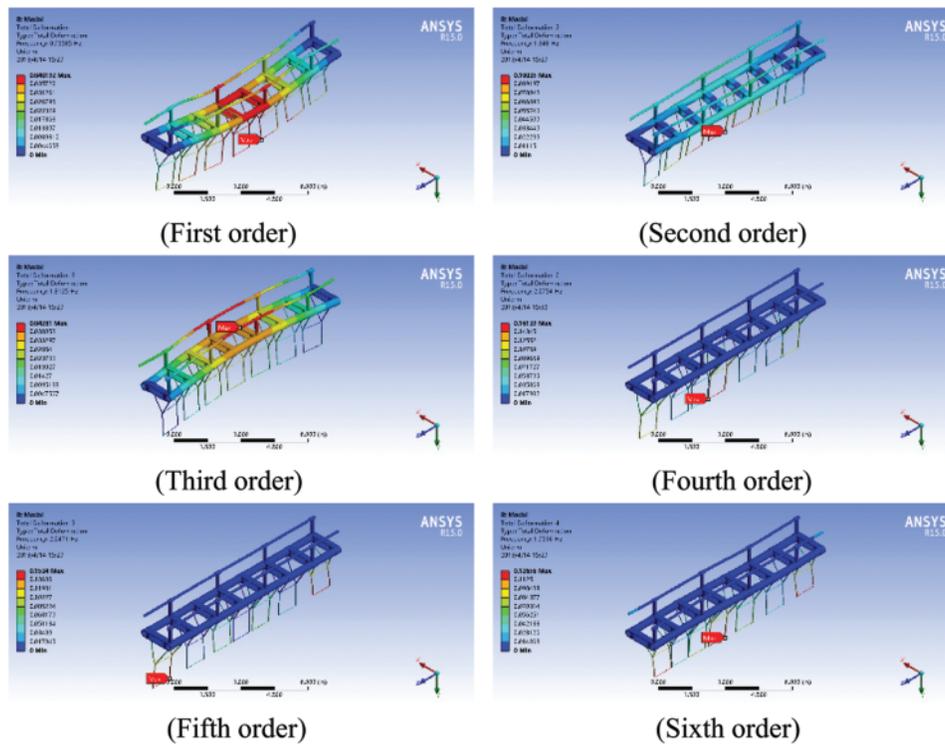
Figure 13: The first six mode shapes of seven units structure

to fix the blade, the beam is the fixed part of the overall structure, and the railing is only a protective structure, and the damage has no excessive influence on the overall performance. In addition, the lower natural frequency is more likely to cause resonance in actual sea conditions, so a smaller number of units should be used.

4.2 Bracket Harmonic Response Analysis

When a fluid load acts on the breakwater structure, the structure generates vibration. The breakwater is a blade in the underwater part, and the cyclic load it receives will be transmitted to the drawbar and cause the overall vibration of the support structure. The tie rod acts as a member for connecting the blade to the bracket and plays an extremely important role in the entire structure.

Under the action of fluid load, the lower end of the tie rod will produce a large displacement, and the connection between the tie rod and the bracket is the most vulnerable part of the structure. Therefore, the load acting on the bracket is simplified to a simple harmonic force with an initial phase angle of zero, the displacement response of the lowermost end of the tie rod and the stress response at the joint of the tie rod and the bracket were analyzed.

In this section, the modal superposition method is used to analyze the harmonic response of different stent lengths and different loads. The modal superposition method is based on modal analysis. The constraints and boundary conditions in the analysis process are the same as in the modal analysis.

4.2.1 Effect of Bracket Length

In order to analyze the influence of the length of the bracket on the response, it is assumed that the force of the blade to the tie rod is uniform in the lateral direction and the amplitude is 5 N/m. The horizontal maximum displacement response, the vertical maximum displacement response, and the maximum stress response at the joint of the lower end of the bracket are calculated as shown in Figs. 14-16.
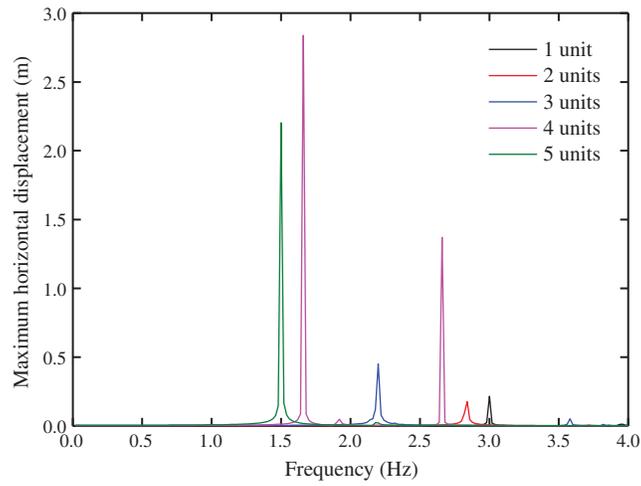
Figure 14: Maximum horizontal displacement for different stent lengths
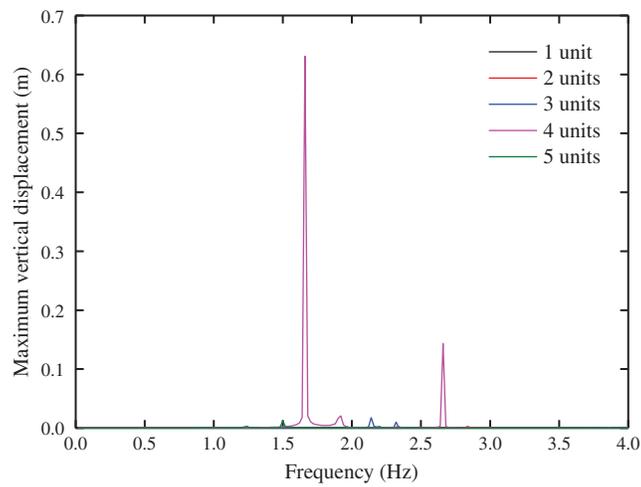
Figure 15: Maximum vertical displacement for different stent lengths
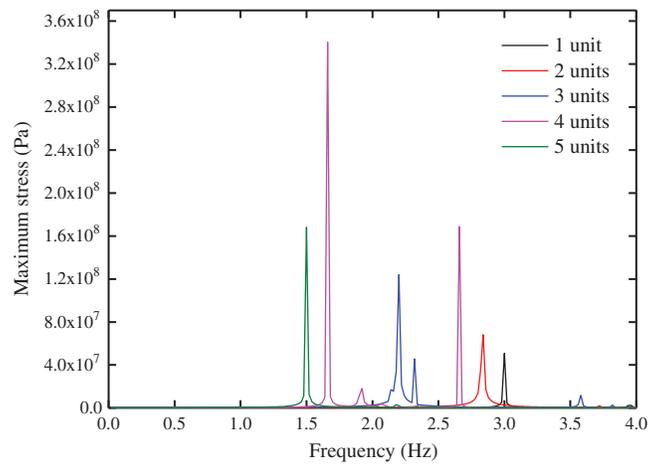
Figure 16: Maximum stress for different stent lengths

As can be seen from Figs. 12-14, the maximum response of displacement and stress occurs at the same frequency. The maximum response of the two units body occurs near the fifth order natural frequency, the maximum response of the three units body occurs near the forth order natural frequency, and the maximum response of the four units and the six units body occurs near the second order natural frequency, the maximum response of the five units body occurs near the first order natural frequency. For both displacement and stress response, the maximum value occurs on the five units structure. The maximum value of the maximum horizontal displacement response and the maximum vertical displacement response is 2.8383 m and 0.6310 m, and the maximum stress at the joint is 340 MPa. It can be seen from Figs. 12 and 13 that when the number of unit bodies is less than 5, the maximum value of the horizontal displacement response is small, but when the number of unit bodies reaches 5, the maximum value of the horizontal displacement response increases significantly. When installing the unit number, select less than 5 unit numbers.

It can be seen from the comparison of the horizontal and vertical displacement responses that the horizontal displacement response is significantly larger than the vertical displacement response, indicating that the tie rod mainly undergoes bending deformation. Therefore, in order to reduce the deformation of the tie rod, corresponding measures should be taken to improve the bending rigidity to prevent damage.

4.2.2 Effect of Load Amplitude

Simulating different sea conditions, the bracket will be subjected to different sizes of ocean waves. Taking the two units body as an example, the magnitude of the load acting on the bracket is changed, and the horizontal, the vertical maximum displacement response of the lower end of the bracket rod and the maximum stress response result at the joint are as shown in Figs. 17-19.
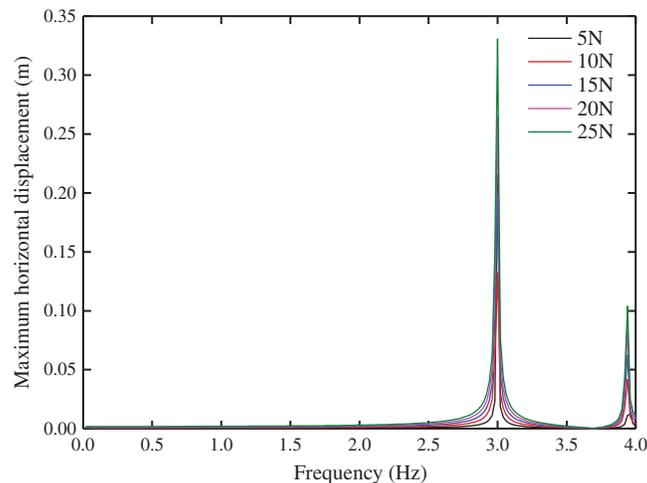
Figure 17: Maximum horizontal displacement at different load amplitudes

It can be seen from Figs. 18-20 that the horizontal displacement response decreases as the angle between the load and the horizontal direction increases, and the vertical displacement response increases. When the angle between the load direction and the horizontal direction is 0° and the excitation frequency is 3 Hz, the maximum stress at the joint is 22.6 MPa.

4.2.3 Effect of Load Angle

In actual sea conditions, the bracket will be tilted in the vertical direction. In order to simulate the response of the bracket at different tilt angles, taking the two-unit body as an example, the applied load amplitude is 5 N/m, and the load angle is changed to obtain the results of Figs. 20-22. It can be seen that
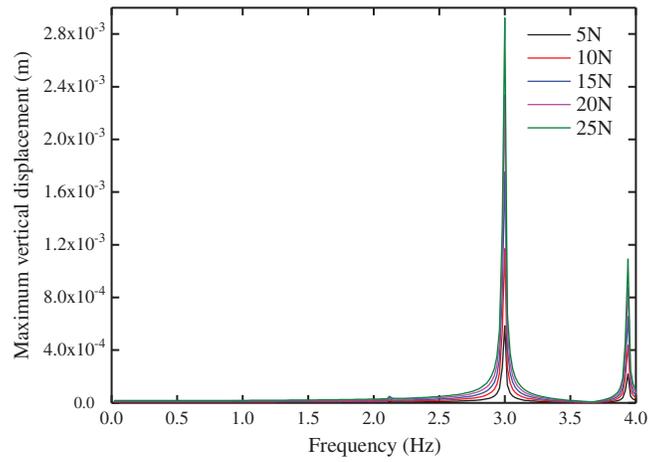
Figure 18: Maximum vertical displacement at different load amplitudes
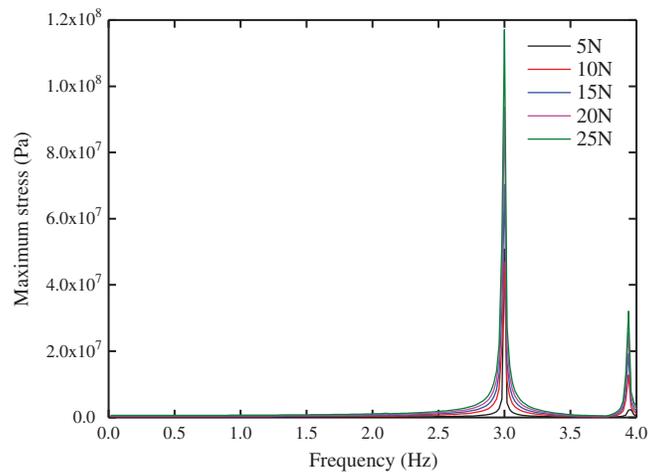
Figure 19: Maximum stress at different load angles
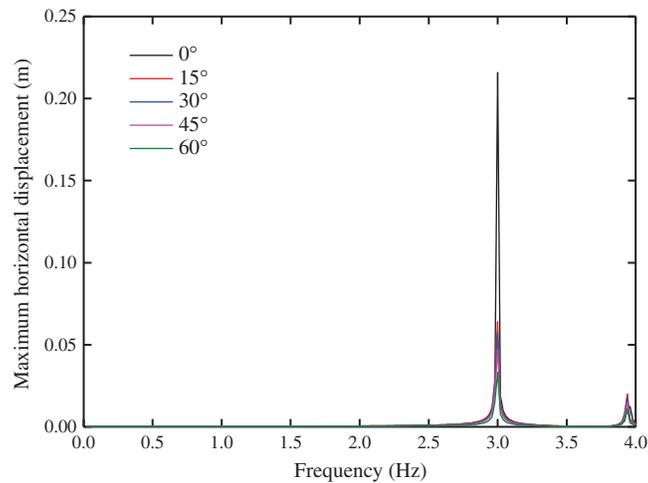
Figure 20: Maximum horizontal displacement at different load angles
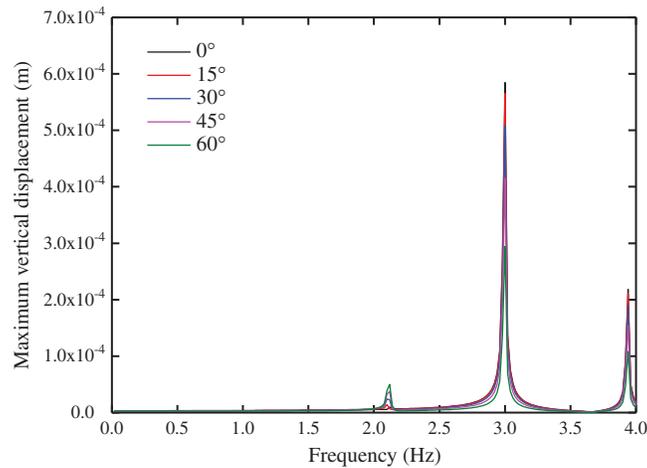
Figure 21: Maximum vertical displacement at different load angles
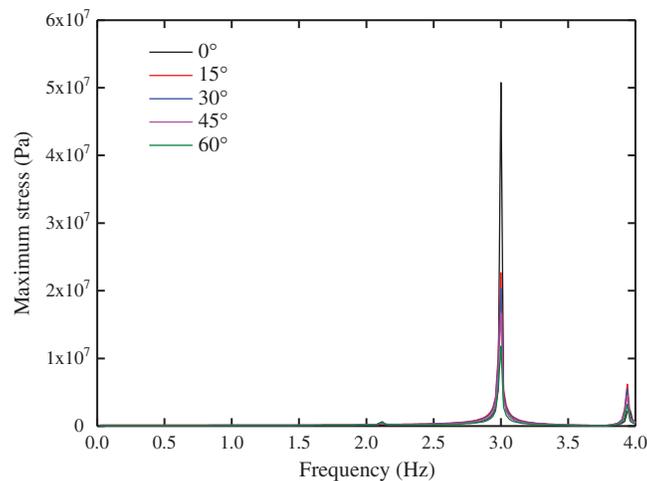
Figure 22: Maximum stress at different load angles

the horizontal displacement response decreases as the angle between the load and the horizontal direction increases, and the vertical displacement response increases. When the angle between the load direction and the horizontal direction is 0° and the excitation frequency is 3 Hz, the maximum stress at the joint is 22.6 MPa.

5 Conclusions

In this paper, a new type of offshore floating breakwater is designed by commercial finite element software geometric modeling. Through the analysis of structural vibration characteristics, the following conclusions are obtained:

1. According to the vibration characteristics analysis of the new offshore floating breakwater structure, the natural frequencies of the blades in the air and in the fluid are quite different. Therefore, the fluid influence must be considered when modal analysis of the structure in the fluid. A more realistic fluid environment can be employed in the further optimization phase of the structure.

2. The tie rod is an important component of the breakwater. The main deformation form is bending deformation. In order to prevent its structural damage, corresponding measures should be taken to improve the bending rigidity of the tie rod and the connection strength of the tie rod-bracket.

3. As the length of the bracket increases, the natural frequency of the structure decreases, the overall flexibility becomes larger, and the main body part and the tie rod are more likely to be damaged. The displacement response at the lowermost end of the tie rod and the maximum stress response at the joint of the tie rod bracket are increased. A small number of unit numbers should be selected as the basic assembly.

Conflicts of Interest: The authors declare that they have no conflicts of interest to report regarding the present study.

References
1. Liu, B. J., Wan, Y., Rao, X. (2018). Structural selection of new floating breakwater. *Journal of Xiamen University of Technology, 26(05),* 57–61.

2. Wang, H., Xu, H. B., Xuan, G. (2013). Hydrodynamic test study on a new type of flexible floating breakwater. *Port Engineering Technology, 50(02),* 10–12.

3. Wang, G. Y., Huang, L., Ren, B., Wang, Y. X. (2014). Theoretical analysis of the performance of wave dissipation of T-type open breakwater. *Advances in Science and Technology of Water Resources, 34(2),* 1–5.

4. Zheng, Y. H., Liu, P. H., Shen, Y. M. (2000). On the radiation and diffraction of linear water waves by an infinitely long rectangular structure submerged in oblique seas. *Ocean Engineering, 34(3/4),* 436–450.

5. Plaut, R. H., Farmer, A. L. (2000). Large motions of a moored floating breakwater modeled as an impact oscillator. *Nonlinear Dynamics, 23(4),* 319–334. DOI 10.1023/A:1008302432739.

6. Wang, Y. X., Wang, G. Y. (2002). Research progress and engineering application of nearshore floating breakwater structure. *Shipbuilding of China, 43,* 314–321.

7. Li, Y. N., Qin, G., Tang, W. X., Zhang, J., Zhang, Z. Z. (2015). Research on dynamic response of deepwater semi-submersible mooring system. *Machine Building & Automation, 44(1),* 209–213.

8. Ma, Z., Cheng, Y., Zhai, G. J. (2017). Hydrodynamic performance of the floating body based on CFD fluid-body interaction theory. *Journal of Ship Mechanics, 21(8),* 950–959.

9. Uzaki, K. I., Ikehata, Y., Matsunaga, N. (2011). Performance of the wave energy dissipation of a floating breakwater with truss structures and the quantification of transmission coefficients. *Journal of Coastal Research, 274(4),* 687–697. DOI 10.2112/JCOASTRES-D-09-00070.1.

10. Liu, Y. Z., Miao, G. P., Li, Y. L., Liu, Z. Y., Liu, H. D. (1997). A time domain computation method for dynamic behavior of mooring system. *Journal of Shanghai Jiaotong University, 31(11),* 7–12.

11. Liu, X. Q., Gu, W. J., Bie, M. J., Zhu, J. K., Wei, J. C. (2015). Analytical solutions of hydrodynamic coefficient for heave motion by an air-floating rectangular box. *Chinese Journal of Applied Mechanics, 32(5),* 1012–1018.

12. Sun, L. P., Niu, Z. Y., Liu, Z. J., Zhang, L. J. (2016). Reactor dynamic response analysis of semi-submersible platform. *Ship Science and Technology, 38(5),* 56–63.

13. Chen, W. M., Fu, Y. Q., Guo, S. X., Jiang, C. H. (2017). A review of fluid-solid coupling and dynamic response of vortex vibration in slender marine cylinders. *Advances in Mechanics, 47,* 201700.

14. Wang, F. M., Li, J., Yang, J. W., Wu, H. J. (2015). Modal and harmonic response analysis of subway gearbox box. *Journal of Mechanical Transmission, 39(9),* 146–150.

15. Michihiro, N. (2007). Numerical study of flow in conical diffuser with vortex generator jets. *Chinese Journal of Mechanical Engineering, 20(01),* 5–9.

16. Wang, G. Y., Liu, D., Ren, B., Wang, Y. X. (2011). Influencing factors of dissipating waves by multiple horizontal plates. *Advances in Science and Technology of Water resources, 31(1),* 33–36.

17. Yang, N., Chen, F., Yi, H., Liu, Y. (2016). Study on the natural frequency of underwater complex stress structures. *Journal of Vibration and Shock, 35(22),* 92–100.

18. Chen, D. Y., Abbas, L. K., Wang, G. P., Rui, X. T. (2017). The influence of flow field environment on the wet mode of flexible riser. *Journal of Harbin Engineering University, 10(38),* 1587–1594.

19. Xiao, J., Zhao, Y. Y., Shu, Y. (2016). Harmonic response analysis of centrifugal impeller under the action of non-cyclic symmetric force. *Journal of Vibration and Shock, 35(23),* 142–147.

20. Chen, Y. F., Chen, W. J., He, Y. L., Zhang, D. X. (2014). Dry and wet modal analysis and evaluation of influencing factors for flexible airship envelop. *Journal of Shanghai Jiaotong University, 48(2),* 1002–1023.

21. Jindal, R., Datta, N. (2015). Free dry and wet vibration of 2-way tapered hollow marine rudder with non-classical pivot: theoretical study. *Proceedings of the ASME, 34th International Conference on Ocean, Offshore and Arctic Engineering, St. John's, Newfoundland, Canada.*

22. Liu, Y., Li, Y. C., Teng, B. (2009). Wave motion over two submerged layers of horizontal thick plates. *Journal of Hydrodynamics, 21(4),* 453–462. DOI 10.1016/S1001-6058(08)60171-7.

23. Hu, H. P., Lu, B. J., Qin, L. P. (2017). The study of effects of pre-stress and fluid-solid interaction effect on vibration properties of underwater shell structures. *Ship Science and Technology, 39(8),* 47–50.

24. Li, X. J., Zhu, H. H., Xu, H. R., Wu, J. D., Xiong, W. (2017). Influence of water medium on vibration mode of ship shaft and paddle combination. *Journal of Wuhan University of Technology (Transportation Science & Engineering), 41(6),* 1005–1012.

25. Gu, C. Z., Zheng, B. L. (2011). Numerical analysis of propeller open-water performance and stress distribution in the blade of ship propeller. *Chinese Quarterly of Mechanics, 32(3),* 440–443.